Biophysical Chemistry 301 (2023) 107080

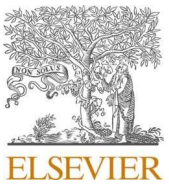

Contents lists available at ScienceDirect

Biophysical Chemistry

journal homepage: www.elsevier.com/locate/biophyschem

Electron paramagnetic resonance spectroscopic characterization of the human KCNE3 protein in lipodisq nanoparticles for structural dynamics of membrane proteins

Matthew W. Scheyer [a], Conner Campbell [a], Patrick L. William [a], Mustakim Hussain [a], Afsana Begum [a], Sebastian Escobar Fonseca [a], Isaac K. Asare [a], Peyton Dabney [a], Carole Dabney-Smith [b], Gary A. Lorigan [b], Indra D. Sahu [a,b,*]

[a] Natural Science Division, Campbellsville University, Campbellsville, KY 42718, USA
[b] Department of Chemistry and Biochemistry, Miami University, Oxford, OH 45056, USA

ARTICLE INFO

Keywords:
Lipodisq nanoparticles/SMALPs
KCNE3
EPR spectroscopy
Membrane mimetic
Membrane proteins
Structural dynamics

ABSTRACT

One of the major challenges in solubilization of membrane proteins is to find the optimal physiological environment for their biophysical studies. EPR spectroscopy is a powerful biophysical technique for studying the structural and dynamic properties of macromolecules. However, the challenges in the membrane protein sample preparation and flexible motion of the spin label limit the utilization of EPR spectroscopy to a majority of membrane protein systems in a physiological membrane-bound state. Recently, lipodisq nanoparticles or styrene-maleic acid copolymer-lipid nanoparticles (SMALPs) have emerged as a membrane mimetic system for investigating the structural studies of membrane proteins. However, its detail characterization for membrane protein studies is still poorly understood. Recently, we characterized the potassium channel membrane protein KCNQ1 voltage sensing domain (KCNQ1-VSD) and KCNE1 reconstituted into lipodisq nanoparticles using EPR spectroscopy. In this study, the potassium channel accessory protein KCNE3 containing flexible N- and C-termini was encapsulated into proteoliposomes and lipodisq nanoparticles and characterized for studying its structural and dynamic properties using nitroxide based site-directed spin labeling EPR spectroscopy. CW-EPR lineshape analysis data indicated an increase in spectral line broadenings with the addition of the styrene-maleic acid (SMA) polymer which approaches close to the rigid limit providing a homogeneous stabilization of the protein-lipid complex. Similarly, EPR DEER measurements indicated an enhanced quality of distance measurements with an increase in the phase memory time (T_m) values upon incorporation of the sample into lipodisq nanoparticles, when compared to proteoliposomes. These results agree with the solution NMR structural structure of the KCNE3 and EPR studies of other membrane proteins in lipodisq nanoparticles. This study along with our earlier studies will provide the reference characterization data that will provide benefit to the membrane protein researchers for studying structural dynamics of challenging membrane proteins.

1. Introduction

Membrane proteins play key roles in localization and organization of the cell and in the cellular function by transferring specific molecules, ions and signals across the cell. Hydrophobic sections of integral membrane protein contain a high fraction of non-polar amino acids and hydrophilic sections contain a high proportion of polar amino acids. The correspondence between hydrophobic regions of protein and the hydrophobic regions of the lipid bilayer, and between the hydrophilic regions of proteins and the extracellular and intracellular environments, stabilizes integral membrane protein within the bilayer. Additionally, integral membrane proteins are stabilized by their interaction with other components of the membrane. Therefore, membrane proteins should be ideally studied in a lipid membrane environment instead of a detergent micelle. Membrane proteins are targets of approximately half of all food and drug administration (FDA) approved modern medical drugs [1,2]. Despite its biological importance, structural dynamics information on membrane bound proteins is still lacking when compared to globular

* Corresponding author at: Natural Science Division, Campbellsville University, Campbellsville, KY 42718, USA.
E-mail address: idsahu@campbellsville.edu (I.D. Sahu).

https://doi.org/10.1016/j.bpc.2023.107080
Received 25 May 2023; Received in revised form 7 July 2023; Accepted 24 July 2023
Available online 26 July 2023

proteins. Electron paramagnetic resonance (EPR) spectroscopy is a powerful biophysical technique for studying structural and dynamic properties of membrane proteins [3–5]. The application of EPR spectroscopy is usually challenging due to difficulties in homogeneous sample preparation of membrane proteins in a functionally relevant membrane-bound state.

Great efforts have been made in the structure biology field for solubilizing membrane proteins for biophysical studies that can maintain the structural and functional activities of the protein. Examples of available membrane mimetics are detergent micelles, bicelles, liposomes, nanodiscs, and lipodisq nanoparticles [6–14]. Each of these membrane mimics have their own pros and cons. Detergent micelles are commonly used to extract membrane protein from the membrane [12]. They can form smaller size micelle complexes suitable for solution nuclear magnetic resonance (NMR) experiments and hence widely used membrane-mimetics for structural studies of membrane proteins. However, due to the lack of lipid bilayers and smaller size and curvature shape of detergent micelles, the structural and functional activities of the protein may get perturbed [15–17]. Bicelles in the form of artificial lipid bilayer discs are composed of a mixture of a long chain and a short chain phospholipids such as 1,2-dimyristoyl-sn-glycero-3- phosphocholine (DMPC) and 1,2-dihexanoyl-*sn*-glycero-3-phosphocholine (DHPC) can be used for the solubilization of membrane proteins providing lipid bilayer environment and accessibility for the interaction of both extracellular and cytoplasmic domains of membrane proteins [18–22]. The disadvantage of using bicelles is that it requires specific types of lipids for bicelle formation that may not maintain the functional activities of all membrane proteins [18,23,24]. Liposomes, or lipid bilayer vesicles, are the closest mimic to native membranes. However, the interior of the vesicle is typically inaccessible to the exterior bulk phase and incorporation of transmembrane proteins often results in a random topology [18]. In addition, incorporation of high concentrations of proteins into liposomes is challenging making spectroscopic EPR studies more difficult [25,26]. Another popular membrane mimetic system that can provide homogeneous protein samples in biomembranes is known as nanodiscs. Nanodiscs are formed by a small patch of lipid bilayer surrounded by two copies of belt-like membrane scaffold protein (MSP) [27]. This method of solubilization helps to boost the phase memory time (T_m) of the EPR spectroscopic samples by minimizing the effect of pockets of high local concentrations of the electron spin [28]. The drawback of this method is the absorbance properties of the membrane scaffold protein that may interfere with the target protein. In addition, this method requires detergent for the incorporation that needs to be completely removed for the formation of the protein and nanodisc complex [29]. Furthermore, the specific scaffold protein-lipid interactions may introduce the challenges in nanodisc sample preparation.

Recently, lipodisq nanoparticles or styrene-maleic acid copolymer-lipid nanoparticles (SMALPs) have been emerged as a promising membrane mimic system that can solubilize membrane proteins in a native like membrane environment for their biophysical studies. Lipodisq nanoparticles are formed by solubilizing a small lipid patch by polymers containing styrene and maleic acid (SMA) at a molar ratio of 3:1 instead of membrane scaffold proteins in a detergent free environment [12,29–34]. The SMA copolymer can solubilize any kind of lipids and maintain the native like lipid composition during the formation of lipodisq nanoparticle complex [35–37]. The lipodisq nanoparticles incorporate one protein molecule per nanoparticle complex with a size of approximately 10–20 nm [14,29,30,38–42]. In the lipodisq nanoparticle complex, membrane proteins can be accessible to their both sides which is appropriate for functional studies [43]. The oligomerization states of membrane proteins are also maintained in lipodisq nanoparticles helping to understand the mechanistic process [44]. Despite a high potential of lipodisq nanoparticles to serve as a better membrane mimetic system for biophysical studies of membrane proteins, their biophysical characterization data in the presence of membrane proteins are still limited [10,30].

In this study, EPR spectroscopy coupled with SDSL is used to investigate the potassium channel accessory protein (KCNE3) in the presence of POPC/POPG lipodisq nanoparticles. KCNE3 is a single transmembrane protein of the KCNE family that modulates the function and trafficking of several voltage gated potassium channels, including KCNQ1 (Q1), and KCNQ4 [45–48]. KCNE3 interacts with KCNQ1 and produces KCNE3/KCNQ1 channels that are voltage-independent in the physiological voltage range, which are important for cardiac action potentials and transport of water and salts across epithelial cells [47,49]. KCNE3 plays a physiological role in repolarization of cardiac action potential. [50] Mutations in KCNE3 leads to several disorders such as long QT syndrome (LQTS), cardiac arrythmia, Brugada syndrome, cystic fibrosis and secretory diarrhea, periodic paralysis, tinnitus, and ménière's disease. [45,50–56] The KCNE3 isotropic bicelles structure consists a curved α-helical transmembrane domain (TMD) with bending being most pronounced near the C-terminal end of the helical TMD, and an extracellular surface associated amphipathic helix in N-terminal, and a short juxtamembrane helix followed by a disordered region in C-terminus. Continuous wave (CW)-EPR and double electron electron resonance (DEER) pulsed EPR spectroscopic experiments were performed on KCNE3 mutants in 1-palmitoyl-2-oleoyl-*sn*-glycero-3-phosphocholine (POPC)/ 1-palmitoyl-2-oleoyl-*sn*-glycero-3-phospho-(1'-*rac*-glycerol) (sodium salt) (POPG) lipid bilayers with 3:1 SMA polymer for the formation of lipodisq nanoparticles system. The EPR spectral lineshape analysis of KCNE3 encapsulated into POPC/POPG lipodisq nanoparticles revealed differences in the spin label side-chain mobility pattern for the spin-labeled KCNE3 residues located within the membrane bilayer region when compared to that for the residues located in the solvent region. The pulse EPR data indicated a significant improvement in the phase memory time (T_m) and DEER distance distribution for the samples in lipodisq nanoparticles when compared to the sample in lipid bilayered vesicles. These results are in well agreement with the structural properties of KCNE3. This study along with our earlier studies will serve as reference database that will be beneficial to researchers using lipodisq nanoparticles/SMALPs as membrane environments.

2. Materials and methods

2.1. Site-directed mutagenesis

The His-tag expression vectors (pET-16b) having a cysteine-less mutant of KCNE3 were transformed into XL10-Gold *Escherichia coli* cells (Agilent). QIAprep Spin Miniprep Kit (Qiagen) was used to extract the plasmid from these cells. Site specific cysteine mutants were introduced into the cysteine-less KCNE3 gene using the QuickChange Lightning Site-Directed Mutagenesis kit (Agilent). The KCNE3 mutations were confirmed by DNA sequencing from XL10-Gold *E. coli* (Stratagene) transformants using the T7 primer (Integrated DNA Technologies). Successfully mutated vectors were transformed into *E.coli* BL21 (DE3) RP Codon-Plus competent cells for protein overexpression. Single spin label mutants (G6C, I76C, and M102C) were generated by introducing Cys residues at the positions (6, 76 and 102). These mutants were chosen to cover N- terminal region, transmembrane domain (TMD) and C-terminal region of KCNE3. Double spin label mutants (S57C/I76C) were generated by introducing pair of Cys residues at the positions (57 and 76).

2.2. Overexpression and purification

The overexpression and purification of BL21 (DE3) RP Codon-Plus *E. coli* cells containing mutated KCNE3 genes were carried out by following a similar protocol described previously [57]. BL21 (DE3) RP Codon-Plus *E.coli* cells carrying mutants of choice were grown in an LB (Luria-Bertani) medium with 100 μg/mL ampicillin and 50 μg/mL chloramphenicol. The cell culture was incubated at 37 °C and 240 rpm until the OD_{600} reached ~0.8. The cell culture was induced using 1 mM IPTG (isopropyl-

1-thio–D-galactopyranoside), followed by continued rotary shaking at 37 °C for ~16 h. Cells were harvested by centrifugation of the cultures at 6500 rpm, for 20 min at 4 °C. The cell pellets were resuspended in 20 mL lysis buffer (70 mM Tris-HCl, Ph 7.8, 300 mM NaCl) per gram of wet pellet, with 1 mM TCEP, lysozyme (0.02 mg/mL), DNase (0.02 mg/mL), RNase (0.02 mg/mL), PMSF (0.2 mg/mL), and magnesium acetate (5 mM) and tumbled at 4 °C for 1 h. The cell suspension was then subjected to sonication for approximately 20 min (5 s on/off cycles, 10 min total on time, Fisher Scientific Sonic Dismembrator Model 500, amplitude 40%) on ice. The lysate was centrifuged at 20,000 ×g for 30 min at 4 °C and the pellet containing inclusion bodies was homogenized with suspension buffer (8 M urea, 25 mM Tris-HCL, 150 mM NaCl, pH 8.0, 1 mM TCEP and 0.2% sodium dodecyl sulfate (SDS) detergent) and rotated overnight at room temperature to solubilize inclusion bodies. After detergent solubilization, the insoluble debris was removed by centrifugation at 20,000 ×g for 30 min at 24 °C. The supernatant was incubated with pre-equilibrated Ni(II)-NTA superflow resin (Qiagen) in suspension buffer for 3 h at room temperature. The protein was then purified using a gravity flow column by washing with 10–12 bed volumes of rinse buffer (25 mM Tris-HCl, 200 mM NaCl, 0.2% SDS, 1 mM TCEP, pH 8.0) to remove non-specific proteins. Resin with bound protein was further washed with 5–6 bed volumes of exchange-rinse buffer (25 mM Tris-HCl, 200 mM NaCl, 0.1% 1-Myristoyl-2-Hydroxy-sn-Glycero-3-Phospho-(1′-rac-Glycerol) (Sodium Salt) (LMPG), 1 mM TCEP, pH 8.0) to produce LMPG micelle samples. Purified His-tagged KCNE3 was eluted in 8 mL of elution buffer (25 mM Tris-HCl, 200 mM NaCl, 250 mM imidazole, 0.1% LMPG, 2 mM TCEP, pH 7.0). Protein samples were concentrated using a Microcon YM-3 (molecular weight cutoff, 3000) filter (Amicon). The protein concentration was determined from the A_{280} using an extinction coefficient of 1.2 mg/mL protein per OD_{280} on a NanoDrop 200c (Thermo Scientific). Sodium Dodecyl Sulfate Polyacrylamide Gel Electrophoresis (SDS-PAGE) was used to confirm protein purity from overexpression.

2.3. Spin labeling and reconstitution into proteoliposomes

Spin labeling and proteoliposomes reconstitution were carried out following the protocol previously described [47]. After purification, each cysteine mutant was concentrated to 0.5 mM. Samples were then reduced with 2.5 mM dithiothreitol (DTT), with gentle agitation at room temperature for 24 h to ensure complete conversion to Cys-SH. 1-oxyl-2,2,5,5-tetramethylpyrroline-3-methylmethanethiosulfonate (MTSL) spin label was added to 10 mM from a 250 mM solution in methanol into 0.5 mM KCNE3 solution, which was then equilibrated at room temperature for 30 min, followed by incubation at 37 °C for 3 h and further incubated overnight at room temperature. Samples were then buffer-exchanged into a 50 mM phosphate, 0.05% LMPG, pH 7.0. Following buffer exchange, samples were bound to Nickel resin in a column, which was then washed with 200 mL of 50 mM phosphate, 0.05% DPC, pH 7.0 to remove excess MTSL. The spin labeled KCNE3 was eluted using elusion buffer ((25 mM Tris-HCl, 200 mM NaCl, 250 mM imidazole, pH 7.0) containing 0.5% DPC or 1% LMPG. The spin-labeling efficiency (~75%) was determined by comparing the nano-drop UV A280 protein concentration with spin concentration obtained from CW-EPR spectroscopy. The spin labeled KCNE3 eluted in the elusion buffer containing 0.5% DPC was used as DPC micelle sample and the spin labeled KCNE3 eluted in the elusion buffer containing 1% LMPG was used as LMPG micelle sample for EPR measurements.

The reconstitution of spin-labeled KCNE3 protein into POPC/POPG (3:1) proteoliposomes was carried out via dialysis methods following a similar protocol in the literature [10,38,47,58,59]. The concentrated spin labeled KCNE3 protein was mixed with a stock lipid slurry (400 mM SDS, 75 mM POPC and 25 mM POPG, 0.1 mM EDTA, 100 mM IMD, pH 7.0). The lipid slurry was pre-equilibrated to clear mixed micelles via an extensive freeze thaw cycles. The final protein:lipid molar ratio was set to 1:400. The KCNE3-lipid mixture was then subjected to extensive dialysis (Spectra/Por Molecularporous Membrane Tubing, 12–14 kD MWCO) to remove all detergent present, during which process KCNE3/POPC/POPG vesicles spontaneously formed. The 4 L dialysis buffer (10 mM imidazole and 0.1 mM EDTA at pH 7.0) was changed twice daily. The completion of detergent removal was determined when the KCNE3-lipid solution became cloudy and the surface tension of the dialysate indicated complete removal of the detergent.

2.4. Reconstitution into DMPC/DPC bicelles

The reconstitution of spin-labeled KCNE3 protein into DMPC/DPC bicelles (3.2:1) was carried out following a similar protocol in literatue [38,60,61]. DMPC powder was added directly to the KCNE3 solubilized in elusion buffer (250 mM IMD, pH 7) containing 0.5% DPC. The bicelles were formed by incubating on ice and 42 °C alternatively with gentle vortexing until the solution becomes clear. The final protein:lipid molar ratio was set to 1:500.

2.5. Reconstitution into POPC/POPG lipodisq nanoparticles

SMA Copolymer (pre-hydrolyzed styrene-maleic anhydride copolymer 3:1 ratio) were purchased from Sigma-Aldrich. The protein-lipid complex was incorporated into SMA-lipodisq nanoparticles following the published protocols [10,29,30,38]. A 500 μl aliquot of proteoliposome-reconstituted protein sample (~30 mM POPC/POPG lipid) was added with equal amount of 2.5% of lipodisq solution prepared in the same dialysis buffer (10 mM IMD, 0.1 mM EDTA at pH 7.0) drop-wise over 3–4 min at a weight ratio 1:1. The protein-lipodisq solution was allowed to equilibrate overnight at 4° C with gentle shaking. The resulting solution was centrifuged at 40,000 ×g for 30 min to remove the non-solubilized protein. The supernatant was further concentrated to desired volume and concentration required for EPR measurements.

2.6. EPR spectroscopic measurements

EPR experiments were conducted at the Ohio Advanced EPR Laboratory. CW-EPR spectra were collected at X-band on a Bruker EMX CW-EPR spectrometer using an ER041xG microwave bridge and ER4119-HS cavity coupled with a BVT 3000 nitrogen gas temperature controller. Each spin-labeled CW-EPR spectrum was acquired by signal averaging 10 42-s field scans with a central field of 3315 G and sweep width of 100 G, modulation frequency of 100 kHz, modulation amplitude of 1 G, and microwave power of 10 mW at different temperatures (296 K -325 K). The spin label side-chain mobility was determined by calculating the inverse central linewidth from each CW-EPR spectrum.

Four pulse DEER experiments were performed using a Bruker ELEXSYS E580 spectrometer equipped with a Super Q-FT pulse Q-band system with a 300 W amplifier and EN5107D2 resonator. All DEER samples were prepared at a spin concentration of 100–120 μM. 30% (*w*/w) deuterated glycerol was used as a cryoprotectant. Approximately 70 μL sample was loaded into a 3 mm inner diameter quartz tube (Wilmad LabGlass, Bucna, NJ) and mounted into the sample holder (plastic rod) inserted into the resonator cavity. The samples were flash frozen with liquid nitrogen just before loading into the resonator cavity. DEER data were collected using the standard four pulse sequence [62] $[(\pi/2)_{\nu 1} - \tau_1 - (\pi)_{\nu 1} - t - (\pi)_{\nu 2} - (\tau_1 + \tau_2 - t) - (\pi)_{\nu 1} - \tau_2 - \text{echo}]$ at Q-band with a probe pulse width of 8/16 ns, pump pulse of 70 ns frequency-swept chirp pulse spanning 85 MHz, shot repetition time of 1000 μs, 100 echoes/point, and 16-step phase cycling at 80 K collected out to ~2.0–3.0 μs for overnight data acquisition time [63]. DEER data were analyzed using MATLAB based DEER Analysis 2015 [64]. The DEER distance distributions $P(r)$ were obtained by Tikhonov regularization [65] in the distance domain, with the constraint $P(r) > 0$. The background correction was obtained by using a homogeneous three-dimensional model for micelle samples and a homogeneous two-dimensional model for bicelles,

liposomes and lipodisq nanoparticles samples. The best fit DEER time domain data was utilized for optimizing the regularization parameter in the L curve.

The spin echo dephasing time or phase memory time (T_m) of spin labels in lipid bilayered vesicles is the measure of the electron spin relaxation in the x-y plane. The dipolar interaction among electron spins and the interaction of electron spins with the nuclear spins of the matrix give rise to the electron spin relaxation. The electron spin relaxation determines the practicability of doing pulse experiments that depend upon echo detection. Transverse relaxation data were collected by using the standard Hahn echo pulse sequence [$(\pi/2)$ - τ_1 - (π) - τ_1-echo] at Q-band with 10/20 ns pulse widths, an initial τ_1 of 200 ns and an increment of 16 ns, 100 echoes/point, and 2-step phase cycling at 80 K. A single exponential decay fitting procedure was used to determine the transverse relaxation time (T_2) or phase memory time (T_m).

2.7. EPR spectral simulations

A non-linear least squares (NLSL) program incorporating the macroscopic order, microscopic disorder (MOMD) model developed by the Freed group was used for the simulation of the EPR spectra [66,67]. Previously published fitting procedure was used to simulate the CW-EPR spectra [38,68]. Principle components of the hyperfine interaction tensor A = [5.5 ± 0.5, 5.4 ± 0.5, 34.8 ± 0.8] G and g-tensors g = [2.0085 ± 0.0002, 2.0069 ± 0.0002, 2.0023 ± 0.0002] were obtained from the literature and tightly refined [38,68]. During the simulation process, the A and g tensors were held constant and the rotational diffusion tensors were varied to obtain best fit simulations. A two-site fit was used to account for both the rigid/slower and higher/faster motional components of the EPR spectrum. A Brownian diffusion model was used to obtain the best fit rotational correlation times and relative population of both motional components.

2.8. Molecular dynamics modeling of KCNE3 keeping MTSL spin labels in POPC/POPG lipid bilayers

Nanoscale molecular dynamics (NAMD) [69] version 2.14 with the CHARMM36 force field was employed to perform molecular dynamics simulations on KCNE3 (PDB ID: 2NDJ) [47] in POPC/POPG lipid bilayers. [70,71] The simulation set up and inputs were generated by using CHARMM-GUI (http://www.charmm-gui.org) [72]. The visual molecular dynamics software (VMD) Xplor version 1.13 [73,74] was used for MD trajectory analysis. The membrane, composed of a pre-equilibrated bilayer of POPC/POPG molecules with a 12,010.5 Å^2 surface, was built using membrane builder protocol under CHARMM-GUI. [72,75] The double MTSL spin labeled KCNE3 (PDB ID: 2NDJ) was inserted into the membrane and the system was solvated into a water box (111.7 Å × 111.5 Å × 67 Å on top and bottom of the membrane surface) and ionized to add bulk water above and below the membrane and to neutralize the system with KCl using the membrane builder protocol [72,75]. The final assembled system comprised waters, POPC/POPG lipids, ions and the protein (a total of 1,74,071 atoms). Six steps of equilibration and minimization of the system were performed under NAMD using the input files generated by CHARMM-GUI before running production run following the instructions provided in the membrane builder protocol. Starting from this equilibrated system, NAMD production run was collected out to 95 ns using Langevin dynamics [76]. Electrostatic interactions were computed using the Particle-Mesh Ewald algorithm with a 12 Å cutoff distance [77] and Van der Waals interactions were computed with a 12 Å cutoff distance and a switching function to reduce the potential energy function smoothly to zero between 10 and 12 Å. Periodic-boundary conditions were used and constant temperature (303K) and pressure (1 atm) were maintained. Equations of motion were integrated with a time step of 2 fs and trajectory data were recorded in 200 ps increments. [76] Probability distance distribution was obtained from trajectory data using the script (distance.tcl) provided in the VMD software package [73]. All molecular dynamics simulations were run on the Miami Redhawk cluster computing facilities at Miami University.

3. Results

We recently characterized the structure of lipodisq nanoparticles in the absence and in the presence of an integral membrane protein KCNE1 using solid-state nuclear magnetic resonance (SSNMR) spectroscopy, dynamic light scattering (DLS), transmission electron microscopy (TEM), and EPR spectroscopy [78–82]. Similarly, we also characterized lipodisq nanoparticles containing the voltage sensing domain of human KCNQ1(Q1-VSD) using EPR spectroscopy [38]. In this study, the lipodisq nanoparticles were further characterized using a spin-labeled membrane protein, human KCNE3. KCNE3, containing a single transmembrane domain with flexible N- and C-termini, was reconstituted into POPC/POPG lipid bilayers. The spin-labeled KCNE3 was investigated using CW-EPR lineshape analysis, pulsed EPR phase memory time (T_m) measurements, DEER distance measurements and side-chain mobility analysis for spin-labeled sites inside and outside of the membrane bilayer. A POPC:POPG (3:1) lipid bilayer was used to mimic phospholipids widely used for studying membrane proteins [10,38,58,83–85]. The gel-to-L$_\alpha$ liquid crystalline phase transition of POPC/POPG is lower than 0 °C [86]. In addition, a 3 to 1 (POPC:POPG) molar ratio mimics the similar level of anionic phospholipids usually found in mammalian cell membranes. [84,86,87]

Figure 1 shows the chemical structure of the MTSL spin-label probe, schematic representation of the predicted topology and amino acid sequence of KCNE3 in lipid bilayers based on previous NMR study [47] and the chemical structure of the SMA polymer.

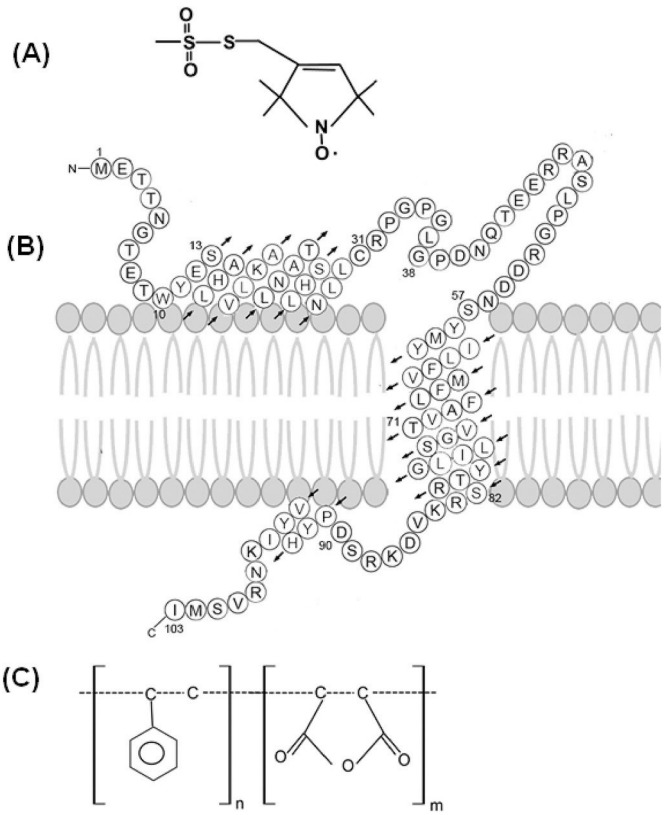

Fig. 1. (A) Chemical structure of the MTSL spin label probe, (B) a predicted topology of KCNE3 in lipid bilayers based on previous solution NMR studies [47], and (C) chemical structure of 3:1 SMA polymer. Chemical structures of MTSL and SMA polymer were prepared using ACD/Sketch (Freeware)-2021.2.1 (www.acdlabs.com).

3.1. Comparison of CW-EPR spectral lineshape data of spin labeled KCNE3 between liposomes and lipodisq nanoparticles

Nitroxide based site-directed spin labeling EPR spectroscopy is a powerful biophysical technique to investigate the structural and dynamic properties of membrane proteins in different membrane mimetic environments. [4,5,68,81,88–93] Three individual amino acid residue positions (G6C on the N-terminus, I76C on the TMD, and M102C on the C-terminus) on KCNE3 were studied using CW-EPR spectroscopy at different temperatures from 296 K to 325 K. CW-EPR spectra of spin-labeled KCNE3 are shown in Figs. 2A-C for the KCNE3 variants G6C on the N-terminus, I76C on the TMD, and M102C on the C-terminus of the membrane in POPC/POPG lipid bilayers (left panel) and POPC/POPG lipodisq nanoparticles (right panel) at temperatures 296 K to 325 K. CW-EPR spectra for the mutant I76C on the TMD show that the spectral line broadening decreases with increase in temperature from 296 K to 325 K in POPC/POPG lipid bilayers. In general, the CW-EPR spectrum of the sample in lipodisq nanoparticles shows broader linewidths having a nearly immobilized shape at 296–297 K, when compared to the EPR spectral lineshape of the sample in POPC/POPG lipid bilayers. However, the spectral line broadening reduces with increasing temperature up to 325 K. Similarly, CW-EPR spectra of the G6C variant on N-terminus shows that the spectral line broadening decreases with increasing temperature from 296 K to 325 K in POPC/POPG lipid bilayers. The CW-EPR spectrum of the sample in lipodisq nanoparticles shows a broader lineshape at 296 K when compared to the EPR spectral lineshape of the sample in POPC/POPG lipid bilayers. However, the spectral linewidths reduce as the temperature is increased up to 325 K. The CW-EPR spectra of the M102C variant indicate that the spectral line broadening reduces with increasing temperature from 296 K to 325

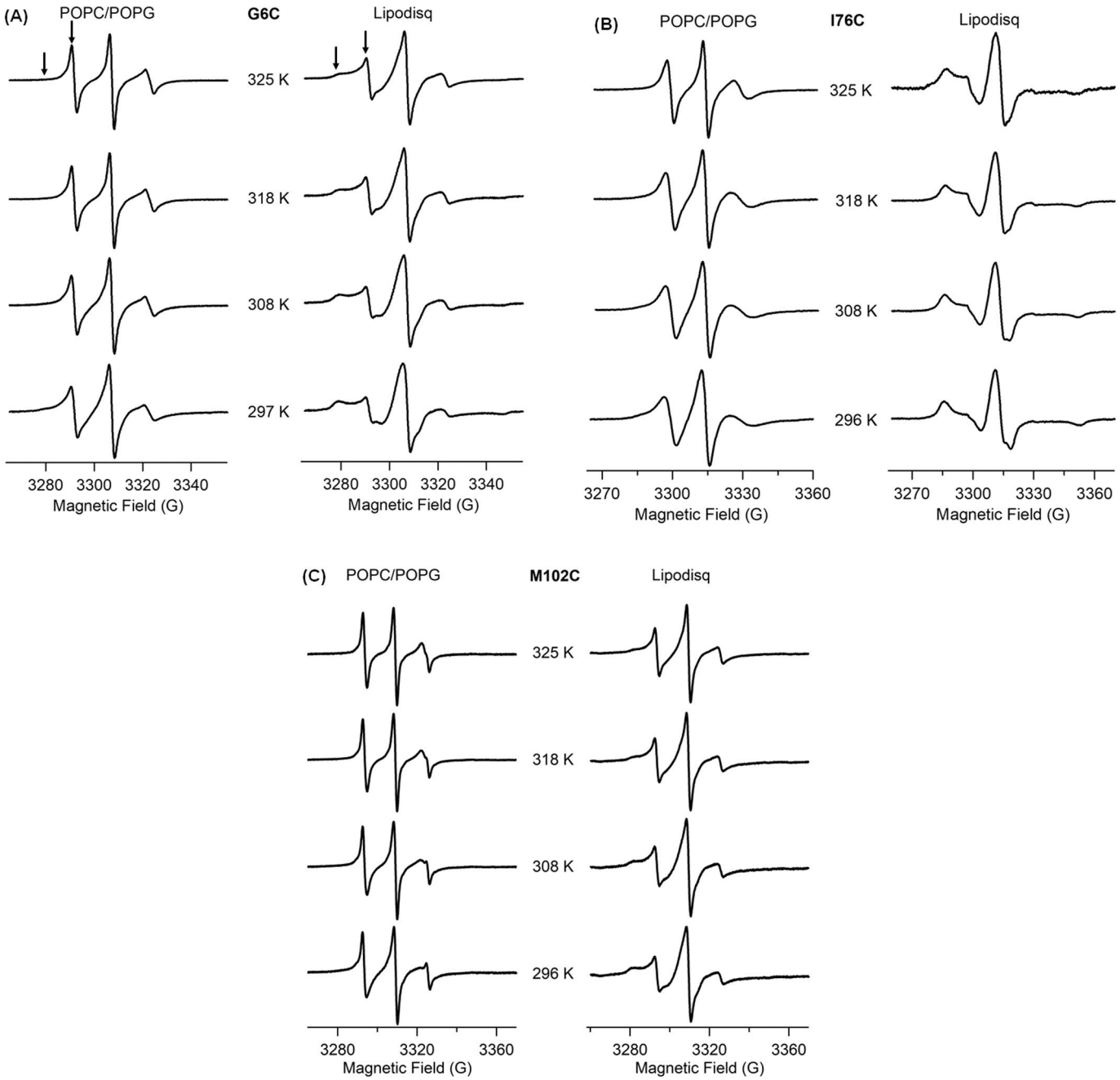

Fig. 2. CW-EPR spectra of spin-labeled KCNE3 at G6C (A), I76C (B), and M102C (C) in POPC/POPG liposomes (left panel) and POPC/POPG lipodisq nanoparticles (right panel) as a function of temperature. The arrows in (A) represent the two motional components in the spectra.

K in POPC/POPG lipid bilayers. Again, the CW-EPR spectrum of the sample in lipodisq nanoparticles also shows a broader lineshape at 296 K, when compared to the EPR spectral lineshape of the sample in POPC/POPG lipid bilayers. However, the EPR spectral linewidths reduces as the temperature increases from 296 K to 325 K.

The EPR spectral linewidth of spin-labeled KCNE3 has a broader component in lipodisq nanoparticles samples when compared to proteoliposome samples, suggesting that the dynamic motion of the spin labeled sites is lower in lipodisq nanoparticle samples. The decrease in the line broadening pattern with increase in temperature for lipodisq nanoparticles samples is consistent with the liposome samples. The two motional components observed in the CW-EPR spectra of all three variants are shown by indicated arrows. The left arrow shows a slower/rigid component and the right arrow shows a more motional/less rigid component. The CW-EPR spectra observed for these spin-labeled KCNE3 samples are in well agreement with previously reported CW-EPR spectra for membrane proteins [38,68,81,84,94,95]. A decrease in the spectral line broadening with increase in temperature is also consistent with the previously reported temperature dependent SDSL CW-EPR spectra [38,81,96,97]. The slower/rigid component is less significant on the spectra of all three sites in POPC/POPG lipid bilayers at higher temperatures 318 K to 325 K. The two motional components of EPR spectra might have averaged at higher temperatures when compared to the spectra collected at 296 K [81]. The alternative explanation may be that the lipid acyl chains may have high fluidity due to the presence of a liquid phase of the POPC/POPG lipid at higher temperature imposing less restrictions to the spin label sites embedded inside the membrane averaging the overall motion of the spin label yielding a single spectral component [98]. The inspection of CW-EPR spectra further indicates that the spin labels at the site I76C on TMD are less dynamic at higher temperatures when compared to that of G6C site on N-terminus and M102C site on C-terminus. Also, the motion of the spin label of M102C is more dynamic when compared to that of N-terminus and TMD sites. This dynamic motion might have imposed an averaging of the motion of the two components at higher temperatures [38,81].

The inverse linewidth of the central line of the EPR spectrum represents the relative mobility of the spin label side-chain and has been widely used as a semi quantitative measure of the nitroxide mobility. [3,5,94,99,100] The inverse central linewidth was plotted against the temperature for all three spin-labeled KCNE3 variants as in Fig. 3. Inspection of Fig. 3 indicates that the inverse central linewidth of the G6C site increases from 0.40 G^{-1} to 0.55 G^{-1} from 296 K to 325 K in liposomes and 0.30 G^{-1} to 0.48 G^{-1} from 296 K to 325 K in lipodisq nanoparticles. Similarly, the inverse central linewidth of the site I76C increases from 0.28 G^{-1} to 0.39 G^{-1} in liposomes and 0.13 G^{-1} to 0.22 G^{-1} in lipodisq nanoparticles from 296 K to 325 K. The inverse central linewidth pattern of the site M102C increases from 0.52 G^{-1} to 0.58 G in liposomes, and 0.40 G^{-1} to 0.50 G^{-1} in lipodisq nanoparticles from 296 K to 325 K. The overall increase in inverse central linewidth pattern for all three sites is similar to the increase in temperature from 296 K to 325 K. However, the inverse central linewidth pattern between liposomes and lipodisq nanoparticle samples for sites G6C and M102C is narrower when compared to that of the site I76C between liposomes and lipodisq nanoparticle samples. This is expected as the lipodisq nanoparticles do not have significant effect or very minor effect on the motion of the spin label probe outside the membrane. [29,30,38,81,82] The inverse central linewidth data also suggest that the motion of the spin label side-chain residue embedded inside the membrane bilayer is more restricted when compared to that of the spin label side-chain residues located outside the membrane bilayer. This motional behavior of the spin label side-chain is in well agreement with previous studies of membrane proteins in lipid bilayers. [38,68,81,85,94,95,101]

To obtain additional insight on the motion of the spin label side-chain of KCNE3, non-linear least squares (NLSL) MOMD EPR spectral simulations were carried out on the representative EPR spectra of spin labeled sites G6C of the N-terminus, I76C of the TMD, and M102C of the C-terminus of KCNE3 at 296 K and 325 K to determine the rotational correlation times of the two motional components and their corresponding relative populations (see Table 1). The EPR spectral simulations under NLSL program were carried out following the previously described method in the literature. [38,66–68,81,82,102–104] The Zeeman interaction tensors (g_{xx}, g_{yy}, g_{zz}) and hyperfine interaction tensors (A_{xx}, A_{yy}, A_{zz}) were held constant during the fitting process and the rotational correlation times (τ) of the two components and their corresponding relative populations were determined from the best fit EPR spectra as shown in Fig. 4 (red lines). Table 1 shows rotational correlation times and the corresponding population of the slower/rigid (site 1) component and the more motional/less rigid component (site 2) of EPR spectra. Two-site fit simulations were employed to obtain the best fit simulations of the EPR spectra at both temperatures 296 K and 325 K. The best fit simulation results showed that the spin label side-chain motion of the site I76C on the TMD at 296 K in POPC/POPG

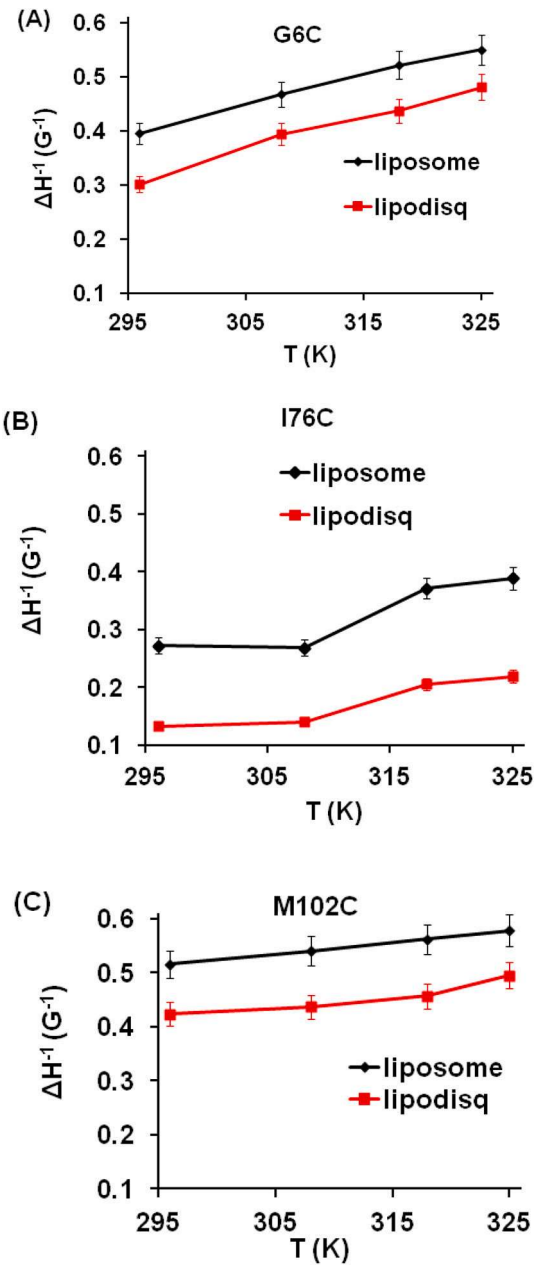

Fig. 3. Inverse central linewidth as a function of temperature for KCNE3 bearing MTSLs at sites G6C (A), I76C (B), and M102C (C) calculated from EPR spectra in Fig. 2.

Table 1
Rotational correlation times (τ) and the relative population (P) of two spectral components of the EPR spectra (Fig. 5) obtained from the best fit NLSL MOMD spectral simulation. The error in correlation time (τ) value is ±0.4–2 ns for liposome samples and ± 0.5–6 ns for lipodisq samples respectively. Similarly, the error in relative population (P) value is +3–6% for liposome samples and ± 4–7% for lipodisq samples. These errors were estimated based on the multiple batch of sample preparation and multiple simulation runs.

		Liposomes				Lipodisq			
Sites	Temperature (K)	τ, ns (site 1)	τ, ns (site 2)	P, % (site 1)	P, % (site 2)	τ, ns (site 1)	τ, ns (site 2)	P, % (site 1)	P, % (site 2)
G6C	297	6.9	2.8	73	27	46	7	63	37
	325	4.2	1.3	80	20	8.3	2.5	77	23
I76C	297	33	2.9	39	61	89	6.9	54	46
	325	18	2.2	31	69	75	5.8	60	40
M102C	297	3.5	1.5	79	21	8.0	1.8	82	18
	325	1.0	0.7	25	81	3.5	1.4	73	27

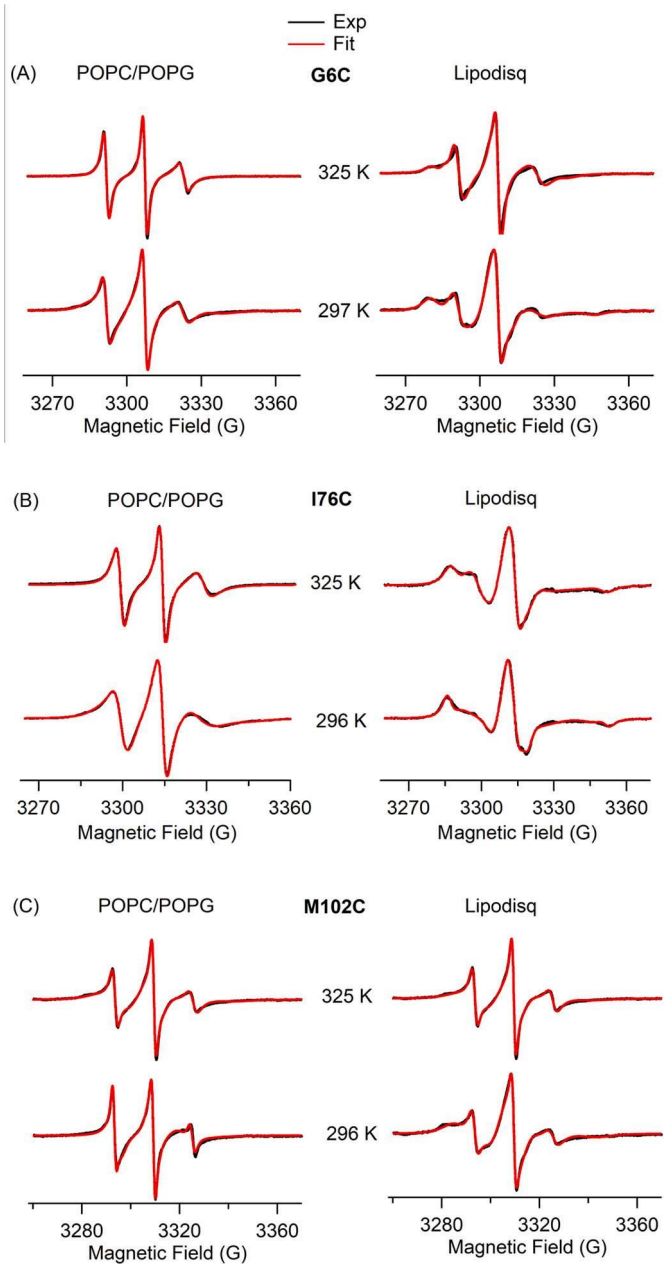

Fig. 4. CW-EPR spectral simulations of KCNE3 variants bearing MTSLs at 296 K and 325 K at the sites G6C (A), I76C (B), and M102C (C) using NLSL MOMD program developed by Freed and Co-workers. [66,67]

liposomes has correlation times of 33 ns for slower/rigid component with a relative population of 39% and 2.9 ns for the more motional/less rigid component with a relative population of 61%, 6.9 ns for the slower/rigid component with a relative population of 73% and 2.8 ns for more motional/less rigid component with a relative population of 27% for the site G6C on N-terminus, while that of the C-terminus variant having 3.5 ns for slower/rigid component with a relative population of 79% and 1.5 ns for the more motional/less rigid component with a relative population of 21% for the site M102C. Similarly, the spin label side-chain motion of KCNE3 variants at 296 K in POPC/POPG lipodisq nanoparticles is closely immobilized with a longer correlation times of 89 ns for the slower/rigid component with a relative population of 54% and 6.9 ns for the more motional/less rigid component with a relative population of 46% for the site I76C, 46 ns for slower/rigid component with a relative population of 63% and 7 ns for the more motional/less rigid component with a relative population of 37% for the site G6C on N-terminus, while that of the C-terminus mutant having 3.5 ns for slower/rigid component with a relative population of 73% and 1.4 ns for the more motional/less rigid component with a relative population of 27% for the site M102C. The simulation results further provided the rotational correlation times decreased to 18 ns for slower/rigid component with a relative population of 31% and 2.2 ns for the more motional/less rigid component with a relative population of 69% for the site I76C, 4.2 ns for slower/rigid component with a relative population of 80% and 1.3 ns for the more motional/less rigid component with a relative population of 20% for the site G6C on N-terminus, while that of the C-terminus mutant decreasing to 1.0 ns for slower/rigid component with a relative population of 77% and 0.7 ns for the more motional/less rigid component with a relative population of 23% for the site M102C with increasing temperature to 325 K in POPC/POPG lipid bilayers. Similarly, the rotational correlation times decreased to 75 ns for the slower/rigid component with a relative population of 60% and 5.8 ns for the more motional/less rigid component with a relative population of 40% for the site I76C of TMD, 4.2 ns for slower/rigid component with a relative population of 80% and 1.3 ns for the more motional/less rigid component with a relative population of 20% for the site G6C on N-terminus, while that of the C-terminal mutant decreased to 3.5 ns for slower/rigid component with a relative population of 73% and 1.4 ns for the more motional/less rigid component with a relative population of 27% for the site M102C with increasing temperature to 325 K in lipodisq nanoparticles. The decrease in the pattern of rotational correlation times for all the lipodisq nanoparticle samples as the temperature increases from 296 K to 325 K is similar to that of the liposome samples. However, the values of the rotational correlation times are longer for lipodisq nanoparticle samples when compared to that of the KCNE3 liposome samples. The slower motional behavior of spin-labeled sites of KCNE3 in lipodisq nanoparticle samples is in well agreement with previous studies. [38,81,82]

3.2. DEER distance measurements on KCNE3 in different membrane mimetic environments

Nitroxide based site-directed spin labeling double electron-electron resonance (SDSL-DEER) spectroscopy is a rapidly growing powerful biophysical technique used to obtain long range distances 18–80 Å for structural studies of bio-macromolecules. [10,62,88,93,105–110] DEER spectroscopy suffers from a short phase memory time (T_m) for the spin-labeled membrane proteins in lipid bilayered vesicles when compared to detergent micelles that introduces challenges in obtaining better quality of DEER distance measurement data. [110–114] The poor phase memory times are due to the packing of the spin-labeled proteins inhomogeneously within the liposomes yielding local inhomogeneous pockets of high spin concentrations [62]. In order to investigate the utilization of lipodisq nanoparticles for pulsed EPR structural studies, a double spin-labeled probe of KCNE3 (S57C-I76C) samples incorporated into various membrane mimetics such as DPC micelles, LMPG micelles, DMPC/DPC bicelles, POPC/POPG lipid bilayers and POPC/POPG

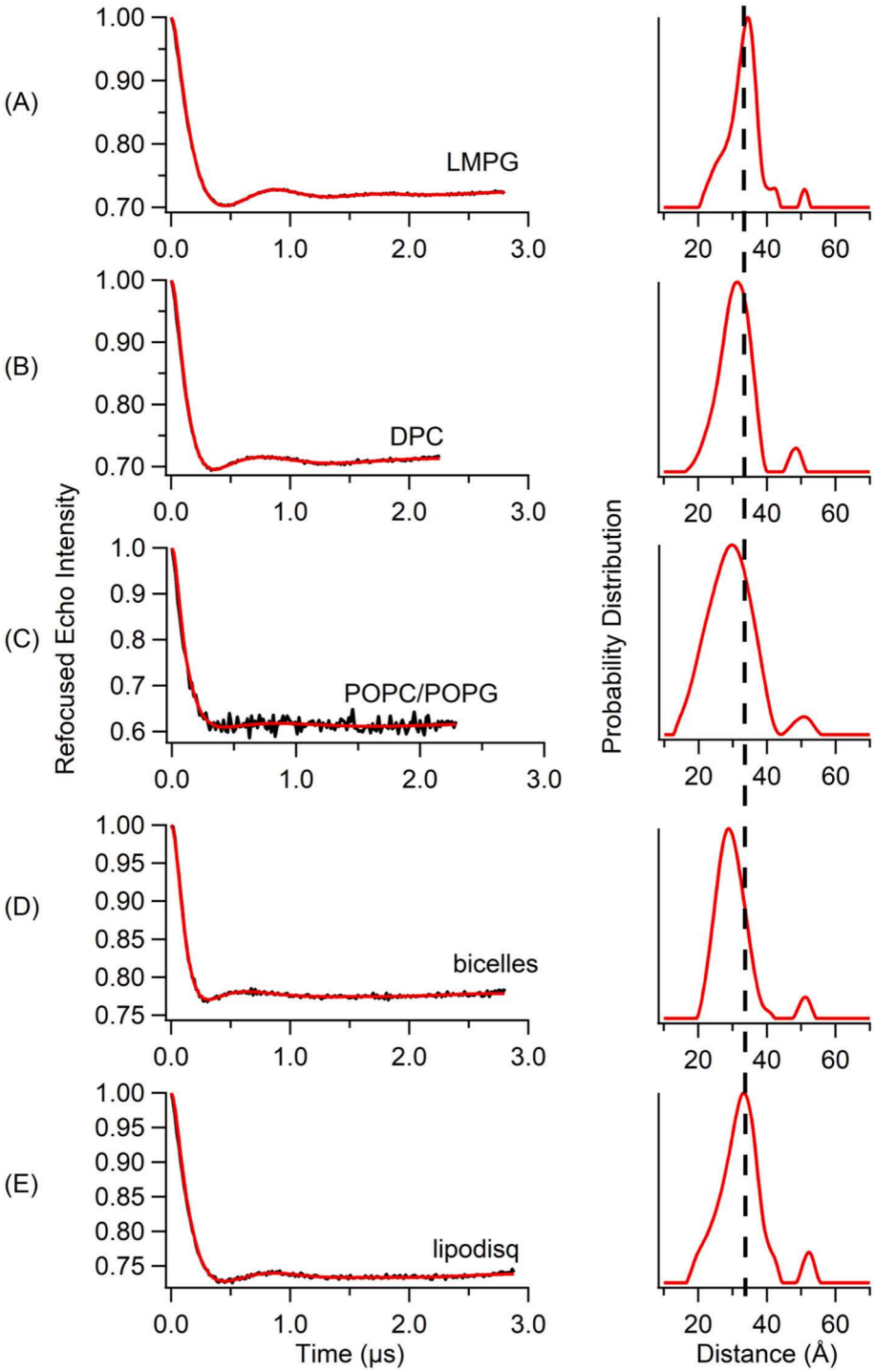

Fig. 5. Q-band DEER data of KCNE3 mutants (S57C/I76C) bearing two MTSL spin labels. Background-subtracted dipolar evolutions of the indicated mutants (left) and their corresponding distance probability distributions from Tikhonov regularization (right) for 1% LMPG micelles (A), 0.5% DPC micelles (B), proteoliposomes (POPC/POPG = 3:1) (C), bicelles (DMPC/DPC = 3.2:1) (D), and lipodisq nanoparticles (E).

lipodisq nanoparticles were subjected to DEER experiments for distance measurements. Fig. 5 shows DEER data for MTSL spin-labeled KCNE3 (S57C/I76C) samples for (A) 1% LMPG micelles, (B) 0.5% DPC micelles, (C) POPC/POPG liposomes, (D) bicelles (DMPC/DPC), and (E) POPC/POPG lipodisq nanoparticles. The time domain traces are shown in the left panel and the distance distributions are shown in the right panel in Figs. 5. Table 2 shows all DEER distances derived from the maximum peak intensity and the approximate full width of the distribution at half maxima (FWHM) from DEER distance measurements on the KCNE3 membrane protein. These distances on KCNE3 are closely matching for each membrane environment within the experimental error and are also consistent with the earlier studies of KCNE3 [47]. These distances data also indicated that the conformations of KCNE3 are closely comparable in all these membrane mimetics utilized in this study. The FWHM for the lipodisq nanoparticles sample (~ 11 Å) is lower than that of the liposome sample (~ 17 Å) and comparable to the micelles (~9 Å) for LMPG samples and ~ 11 Å for DPC sample) and bicelles (~11 Å) samples. These DEER data also indicated that the signal-to-noise ratio (S/N) of DEER time domain data is significantly improved for lipodisq nanoparticles having well defined oscillations with a longer data acquisition time out to ~3 μs when compared to the POPC/POPG lipid bilayers (~2.5 μs). This improvement in the S/N of the lipodisq nanoparticle sample is due to the improvement in the value of the phase memory time (T_m) for the lipodisq nanoparticles sample when compared to the liposomes sample. In order to validate the experimental results, molecular dynamics modeling of KCNE3 bearing two MTSL spin labels (S57C/I76C) was performed in POPC/POPG lipid bilayers using nanoscale molecular dynamics (NAMD) version 2.14 with the CHARMM36 force field. [69–71] A 95 ns molecular dynamics simulation data revealed (32 ± 3) Å distance (Fig. 6) which is closely agreed with the experimental values in different membrane environments within the experimental error.

In order to understand the effect of lipodisq nanoparticles on the *Tm*-values, the representative T_m-curves for the double spin labeled KCNE3 (S57C/I76C) for POPC/POPG lipid bilayers and lipodisq nanoparticles samples were plotted in Fig. 7. The phase memory time (T_m) data were analyzed using similar method published in the literature. [10,38,81] Fig. 7 clearly showed the signal intensity at a specific decay time of 3 μs (commonly used data acquisition time) is higher by ~2 fold for the lipodisq nanoparticles sample when compared to the liposomes sample. The single exponential decay fitting method could not adequately fit the T_m data sets for direct comparison of T_m values for different samples. However, qualitatively the T_m values of the lipodisq nanoparticles KCNE3 samples have increased by a factor of ~2 when compared to KCNE3 in liposomes sample. The increased phase memory time helps to extend the DEER measurements for longer range of distances with better signal-to-noise ratio (S/N) of the time domain DEER data.

4. Discussions

Biologically pertinent lipid bilayer membranes help to stabilize membrane protein structure and functions. Homogeneously prepared liposome samples are very essential to achieve better experimental EPR data quality for the quantitative information about the structural dynamics of membrane proteins. An increased line broadening was observed in the CW-EPR spectra of the lipodisq nanoparticle samples in comparison to the liposome samples suggesting a decrease in the spin label side-chain motion for the lipodisq nanoparticle samples when compared to the liposome samples. The increasing spectral line broadening behavior is consistent with the published EPR studies of membrane proteins [29,38,81,82,115,116]. The interaction of the SMA polymer with the lipid acyl chain generates lateral pressure while isolating the small specific size of the lipid-protein complex in the formation of the lipodisq nanoparticles system [29]. This lateral pressure may provide additional restriction to the spin label side chain of the incorporated protein reducing its dynamic motion. The earlier

Table 2
The four pulse major peak distance and approximate full width of the distribution at half maxima (FWHM) from DEER distance measurements on the KCNE3 membrane protein. The uncertainties for these distances are =2–4 Å.

Membrane Mimetic	KCNE3 Double Mutant (S57C/I76C)	
	Distance (Å)	FWHM (Å)
LMPG Micelles	34	~9
DPC Micelles	31	~11
POPC/POPG Lipid Bilayers	30	~17
DMPC/DPC Bicelles	29	~11
POPC/POPG Lipodisq	34	~11

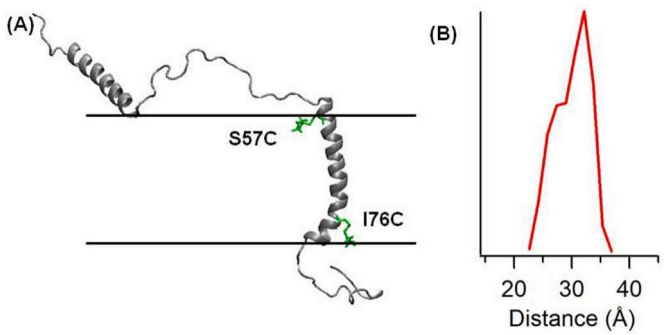

Fig. 6. Cartoon representation of the KCNE3 (PDB ID: 2M9Z) [47] bearing two MTSL spin labels at S57C and I76C **(A)** and corresponding distance distribution obtained from 95 ns molecular dynamics trajectory data analysis **(B).** The solid lines represent the lipid bilayer interface.

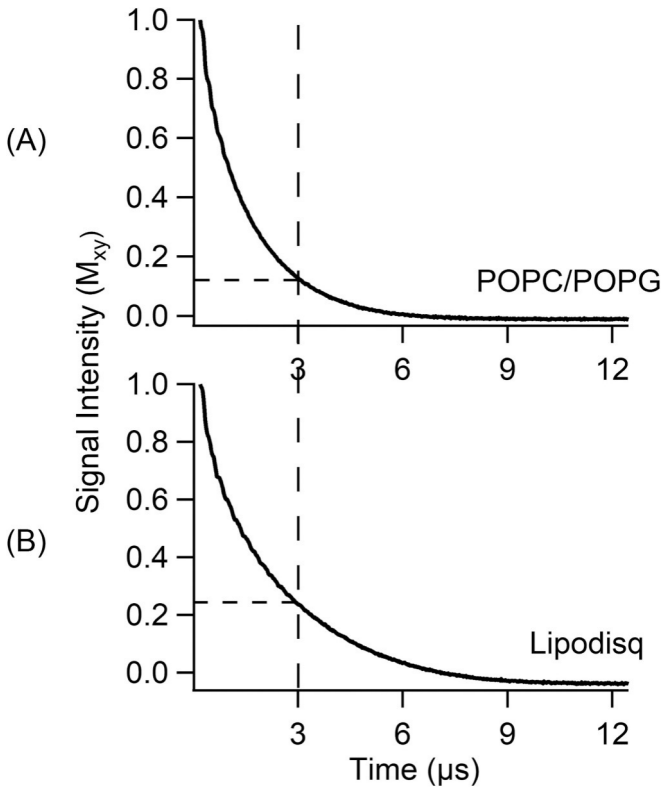

Fig. 7. Experimental phase memory curves for double spin labeled KCNE3 mutants (S57C/I76C) bearing two MTSL spin labels for liposomes (POPC/POPG = 3:1) (A), and POPC/POPG lipodisq nanoparticles (B). The T_m values are (1.2 ± 0.2) μs for liposomes and (2.0 ± 0.2) μs for lipodisq nanoparticles.

biophysical studies performed by Jamshad et al. has reported that the SMA polymer takes the form of bracelet surrounding the lipid membrane in which the styrene moieties interact directly with the lipid acyl chain aligned parallel to the membrane normal and the maleic acid groups interact with the lipid head groups aligned in the same direction of the styrene moieties [116]. The decrease in the motion of the lipid acyl chain during the formation of the lipodisq nanoparticles may be due to the driving force towards the burial of the styrene moieties into the hydrophobic core of the membrane [116]. During the formation of the lipodisq nanoparticles, the SMA polymers may extract the patches of membrane having well incorporated membrane protein and stabilizes the specific small sizes [37]. Additionally, the outside spin label probe has also reduced motion in the presence of lipodisq nanoparticles when compared to that of the liposomes due to the overall increase in the viscosity of the solution during the formation of lipodisq nanoparticles system (see Fig. 2). [29,30] A significant differences in the inverse central linewidth pattern between the spin label probe inside the membrane and the spin label probe outside the membrane was also observed in this study (see Fig. 3). This pattern is also consistent with our previous studies. [38,82]

In previous studies, we showed that the lipodisq nanoparticles based sample preparation of the single transmembrane KCNE1 protein, the influenza A M2 protein, and potassium channel voltage sensing domain (KCNQ1-VSD) revealed significant improvement in signal-to-noise ratio (S/N) for DEER time domain data and boosted the phase memory time by ~2-fold. [10,38,59,117] In this study, EPR measurements on the potassium channel accessory protein KCNE3 having single pass transmembrane section containing flexible N- and C-termini also showed significant improvement in signal-to-noise ratio (S/N) for DEER time domain data with the phase memory time increased by ~2-fold for lipodisq nanoparticle samples. The major peak DEER distances obtained from the probability distribution plots (Fig. 5 (right panel)) for the doubly spin-labeled mutant of KCNE3 (S57C/I76C) in different membrane environments including 1% LMPG micelles, 0.5% DPC micelles, POPC/POPG liposomes, DMPC/DPC bicelles and POPC/POPG lipodisq nanoparticles are close to each other within the experimental error suggesting that the structural perturbation of the protein due to the formation of lipodisq nanoparticles is not significant. [10,38,59,81,82] Recent studies by Kroncke et al. reported that the DEER distances obtained between two spin labeled sites on KCNE3 (S57C/S82C) are similar in different membrane environments including (lyso-myristoylphosphatidylcholine (LMPC) micelles, bicelles (DMPG/DHPC), and POPC/POPG lipid bilayers. [47] The DEER distances obtained on the KCNE3 (S57C/I76C) in different membrane environments are also consistent with the 95 ns molecular dynamics simulation distance data (see Fig. 7B). Recent studies on lipodisq nanoparticle systems from several research laboratories have reported that the formation of lipodisq nanoparticles doesn't cause any significant changes in the functional activities of the protein systems. [30,37,118] There is no significant restriction applied by the SMA polymer to the encapsulated protein in lipodisq nanoparticles, and hence the natural membrane environment of the protein is maintained during biophysical measurements. [37] The decrease in the overall motion of the lipid-protein complex is useful in determining the local motional dynamics of the spin-label probe. [103] Recent studies have suggested the significant presence of SMA polymers at the lipid head groups during the formation of SMALPs that may perturb structure and dynamics of lipid and the possibly of the incorporated proteins [119,120].

The lipodisq nanoparticle sample preparation protocol optimized for EPR spectroscopic studies in this study is consistent with our earlier optimized lipodisq nanoparticle sample preparations for the SSNMR, TEM and EPR spectroscopic studies. [10,38,59,78,80,81] In the lipodisq nanoparticles based samples, the protein molecules are organized independently from each other due to smaller and homogeneous sizes of lipodisq nanoparticles. This results in an even distribution of the spin-labels leading to a reduction in the local spin concentration that induces an increase in the phase memory time for DEER experimental measurements. [10,30,59,80] The enhancement in the phase memory time favors longer DEER distance measurements more precisely and also boosts the S/N of the time domain DEER data for structural studies of challenging membrane proteins. The improvement in the phase memory time is well agreed with the previously published phase memory time of membrane proteins in lipodisq nanoparticles. [10,38,59,81] The increasing amount of CW-EPR spectral lineshape broadening and phase memory time (T_m) for lipodisq nanoparticle samples observed in this study may vary based on the types of membrane protein systems, and the length and choice of phospholipids under the study [121]. Recently, several derivatives of the SMA copolymers have been utilized to improve the data quality of the biophysical studies of membrane proteins. [33,122–125] Based on our current and previous studies, [10,38,41,59,78,81,82,117] we speculate that the lipodisq nanoparticles system is a very good membrane environment and beneficial for EPR structural and dynamic studies of wide ranges of membrane proteins. We also suggest EPR studies of additional protein systems and lipid systems need to be conducted to further generalize the utility of lipodisq nanoparticles.

5. Conclusion

A single pass potassium channel accessory protein human KCNE3 encapsulated into lipodisq nanoparticles was studied using nitroxide based site-directed spin labeling EPR spectroscopy. An increase in the CW-EPR spectral line broadening was obtained for the spin labeled KCNE3 mutants in lipodisq nanoparticles when compared to that in liposomes. The DEER spectroscopic results showed a significant improvement in the signal-to-noise ratio (S/N) for DEER time domain data with the phase memory time boosted by ~2-fold for lipodisq nanoparticle samples. The lipodisq nanoparticle based samples providing longer phase memory time can favor longer DEER distance measurements more precisely for structural studies of complicated membrane proteins. The results of this study and our earlier studies provide a reference database and will be very helpful for researchers working on EPR structural dynamic studies of more complicated membrane protein systems.

All authors have approved the manuscript submission.

Declaration of Competing Interest

The authors declare that they have no known competing financial interests or personal relationships that could have appeared to influence the work reported in this paper.

Acknowledgement

We would also like to appreciate Dr. Jens Mueller, the Facility Manager, Redhawk Cluster Miami University, for assistance with the computational work. This work is generously supported by National Science Foundation NSF MCB-2040917 award. Gary A. Lorigan would like to acknowledge support from NSF (MRI-1725502) grant, NIGMS/NIH Maximizing Investigator's Research Award (MIRA) R35 GM126935 award, the Ohio Board of Regents, and Miami University. Gary A. Lorigan would also like to acknowledge support from the John W. Steube Professorship. Carole Dabney-Smith would like to acknowledge support from the NIGMS/NIH R15 GM137251 and the Ernest H. Volwiler Professorship. Mathew Scheyer would also like to acknowledge support from Appalachian College Association Ledford Scholars Program.

References

[1] J.P. Overington, B. Al-Lazikani, A.L. Hopkins, How many drug targets are there? Nat. Rev. Drug Discov. 5 (12) (2006) 993–996.

[2] C.R. Sanders, J.K. Myers, Disease-related misassembly of membrane proteins, Annu. Rev. Biophys. Biomol. Struct. 33 (2004) 25–51, https://doi.org/10.1146/annurev.biophys.33.110502.140348.
[3] W.L. Hubbell, H.S. McHaourab, C. Altenbach, M.A. Lietzow, Watching proteins move using site-directed spin labeling, Structure 4 (7) (1996) 779–783.
[4] C.S. Klug, J.B. Feix, Methods and applications of site-directed spin labeling EPR spectroscopy, Methods Cell Biol. 84 (2008) 617–658.
[5] I.D. Sahu, R.M. McCarrick, G.A. Lorigan, Use of electron paramagnetic resonance to solve biochemical problems, Biochemistry 52 (2013) 5967–5984.
[6] A.M. Seddon, P. Curnow, P.J. Booth, Membrane proteins, lipids and detergents: not just a soap opera, Bba-Biomembranes 1666 (1–2) (2004) 105–117.
[7] S.H. Park, S.J. Opella, Triton X-100 as the "short-chain lipid" improves the magnetic alignment and stability of membrane proteins in phosphatidylcholine bilayers for oriented-sample solid-state NMR spectroscopy, J. Am. Chem. Soc. 132 (36) (2010) 12552–12553.
[8] A.A. De Angelis, S.J. Opella, Bicelle samples for solid-state NMR of membrane proteins, Nat. Protoc. 2 (10) (2007) 2332–2338.
[9] T.H. Bayburt, S.G. Sligar, Membrane protein assembly into nanodiscs, FEBS Lett. 584 (9) (2010) 1721–1727.
[10] I.D. Sahu, R.M. McCarrick, K.R. Troxel, R. Zhang, H.J. Smith, M.M. Dunagan, M. S. Swartz, P.V. Rajan, B.M. Kroncke, C.R. Sanders, et al., DEER EPR measurements for membrane protein structures via bifunctional spin labels and lipodisq nanoparticles, Biochemistry 52 (38) (2013) 6627–6632.
[11] T.H. Bayburt, S.G. Sligar, Self-assembly of single integral membrane proteins into soluble nanoscale phospholipid bilayers, Protein Sci. 12 (11) (2003) 2476–2481.
[12] A. Colbasevici, N. Voskoboynikova, P.S. Orekhov, M.E. Bozdaganyan, M. G. Karlova, O.S. Sokolova, J.P. Klare, A.Y. Mulkidjanian, K.V. Shaitan, H. J. Steinhoff, Lipid dynamics in nanoparticles formed by maleic acid-containing copolymers: EPR spectroscopy and molecular dynamics simulations, Biochim. Biophys. Acta-Biomembr. 1862 (5) (2020), 183207.
[13] S.C. Lee, S. Khalid, N.L. Pollock, T.J. Knowles, K. Edler, A.J. Rothnie, O.R. T. Thomas, T.R. Dafforn, Encapsulated membrane proteins: a simplified system for molecular simulation, Biochim. Biophys. Acta-Biomembr. 1858 (10) (2016) 2549–2557.
[14] I.D. Sahu, G.A. Lorigan, Role of membrane mimetics on biophysical EPR studies of membrane proteins, BBA - Biomembr. 1865 (2023), 184138.
[15] J.N. Sachs, D.M. Engelman, Introduction to the membrane protein reviews: the interplay of structure, dynamics, and environment in membrane protein function, Annu. Rev. Biochem. 75 (2006) 707–712.
[16] G.G. Privé, Detergents for the stabilization and crystallization of membrane proteins, Methods 41 (4) (2007) 388–397.
[17] R.M. Garavito, S. Ferguson-Miller, Detergents as tools in membrane biochemistry, J. Biol. Chem. 276 (35) (2001) 32403–32406.
[18] T. Raschle, S. Hiller, M. Etzkorn, G. Wagner, Nonmicellar systems for solution NMR spectroscopy of membrane proteins, Curr. Opin. Struct. Biol. 20 (4) (2010) 471–479.
[19] T.-L. Lau, C. Kim, M.H. Ginsberg, T.S. Ulmer, The structure of the integrin alpha IIb beta 3 transmembrane complex explains integrin transmembrane signalling, EMBO J. 28 (9) (2009) 1351–1361.
[20] D. Lee, K.F.A. Walter, A.-K. Brueckner, C. Hilty, S. Becker, C. Griesinger, Bilayer in small bicelles revealed by lipid-protein interactions using NMR spectroscopy, J. Am. Chem. Soc. 130 (42) (2008) 13822–13823.
[21] C.R. Sanders, R.S. Prosser, Bicelles: a model membrane system for all seasons? Struct. Fold. Design 6 (10) (1998) 1227–1234.
[22] Z. Lu, W.D. Van Horn, J. Chen, S. Mathew, R. Zent, C.R. Sanders, Bicelles at low concentrations, Mol. Pharm. 9 (4) (2012) 752–761.
[23] R.R. Vold, R.S. Prosser, Magnetically oriented phospholipid bilayered micelles for structural studies of polypeptides. Does the ideal bicelle exist? J. Magn. Reson. Ser. B 113 (3) (1996) 267–271.
[24] U.H.N. Duerr, M. Gildenberg, A. Ramamoorthy, The magic of Bicelles lights up membrane protein structure, Chem. Rev. 112 (11) (2012) 6054–6074.
[25] E.R. Geertsma, N.A.B.N. Mahmood, G.K. Schuurman-Wolters, B. Poolman, Membrane reconstitution of ABC transporters and assays of translocator function, Nat. Protoc. 3 (2) (2008) 256–266.
[26] G. Fang, R. Friesen, F. Lanfermeijer, A. Hagting, B. Poolman, W.N. Konings, Manipulation of activity and orientation of membrane-reconstituted di-tripeptide transport protein DtpT of Lactococcus lactis, Mol. Membr. Biol. 16 (4) (1999) 297–304.
[27] I.G. Denisov, S.G. Sligar, Nanodiscs for structural and functional studies of membrane proteins, Nat. Struct. Mol. Biol. 23 (6) (2016) 481–486.
[28] P. Zou, H.S. McHaourab, Increased sensitivity and extended range of distance measurements in spin-labeled membrane proteins: Q-band double electron-electron resonance and nanoscale bilayers, Biophys. J. 98 (6) (2010) L18–L20.
[29] M.C. Orwick, P.J. Judge, J. Procek, L. Lindholm, A. Graziadei, A. Engel, G. Gröbner, A. Watts, Detergent-free formation and physicochemical characterization of nanosized lipid-polymer complexes: lipodisq, Angew. Chem.-Intern. Ed. 51 (19) (2012) 4653–4657.
[30] M. Orwick-Rydmark, J.E. Lovett, A. Graziadei, L. Lindholm, M.R. Hicks, A. Watts, Detergent-free incorporation of a seven-transmembrane receptor protein into nanosized bilayer lipodisq particles for functional and biophysical studies, Nano Lett. 12 (9) (2012) 4687–4692.
[31] T.J. Knowles, R. Finka, C. Smith, Y.-P. Lin, T. Dafforn, M. Overduin, Membrane proteins solubilized intact in lipid containing nanoparticles bounded by styrene maleic acid copolymer, J. Am. Chem. Soc. 131 (22) (2009) 7484–7485.
[32] M. Jamshad, Y.-P. Lin, T.J. Knowles, R.A. Parslow, C. Harris, M. Wheatley, D. R. Poyner, R.M. Bill, O.R.T. Thomas, M. Overduin, et al., Surfactant-free purification of membrane proteins with intact native membrane environment, Biochem. Soc. Trans. 39 (2011) 813–818.
[33] J.M. Dorr, S. Scheidelaar, M.C. Koorengevel, J.J. Dominguez, M. Schafer, C.A. van Walree, J.A. Killian, The styrene-maleic acid copolymer: a versatile tool in membrane research, Europ. Biophys. J.: EBJ 45 (1) (2016) 3–21.
[34] M. Overduin, M. Esmaili, Structures and interactions of transmembrane targets in native Nanodiscs, Slas Discov. 24 (10) (2019) 943–952.
[35] S. Scheidelaar, M.C. Koorengevel, J.D. Pardo, J.D. Meeldijk, E. Breukink, J. A. Killian, Molecular model for the Solubilization of membranes into Nanodisks by styrene maleic acid copolymers, Biophys. J. 108 (2) (2015) 279–290.
[36] A.R. Long, C.C. O'Brien, K. Malhotra, C.T. Schwall, A.D. Albert, A. Watts, N. N. Alder, A detergent-free strategy for the reconstitution of active enzyme complexes from native biological membranes into nanoscale discs, BMC Biotechnol. 13 (2013) 41.
[37] C. Logez, M. Damian, C. Legros, C. Dupre, M. Guery, S. Mary, R. Wagner, C. M'Kadmi, O. Nosjean, B. Fould, et al., Detergent-free isolation of functional G protein-coupled receptors into Nanometric lipid particles, Biochemistry 55 (1) (2016) 38–48.
[38] I.D. Sahu, G. Dixit, W.D. Reynolds, R. Kaplevatsky, B.D. Harding, C.K. Jaycox, R. M. McCarrick, G.A. Lorigan, Characterization of the human KCNQ1 voltage sensing domain (VSD) in Lipodisq nanoparticles for Electron paramagnetic resonance (EPR) spectroscopic studies of membrane proteins, J. Phys. Chem. B 124 (12) (2020) 2331–2342.
[39] I.D. Sahu, R. Zhang, M.M. Dunagan, A. Craig, A., L. G., Characterization of KCNE1 inside lipodisq nanoparticles for EPR spectroscopic studies of membrane proteins, J. Phys. Chem. B 121 (21) (2017) 5312–5321.
[40] I.D. Sahu, R.M. McCarrick, K.R. Troxel, R.F. Zhang, H.J. Smith, M.M. Dunagan, M.S. Swartz, P.V. Rajan, B.M. Kroncke, C.R. Sanders, et al., DEER EPR measurements for membrane protein structures via bifunctional spin labels and lipodisq nanoparticles, Biochemistry 52 (38) (2013) 6627–6632.
[41] R.F. Zhang, I.D. Sahu, A.P. Bali, C. Dabney-Smith, G.A. Lorigan, Characterization of the structure of lipodisq nanoparticles in the presence of KCNE1 by dynamic light scattering and transmission electron microscopy, Chem. Phys. Lipids 203 (2017) 19–23.
[42] K.S. Simon, N.L. Pollock, S.C. Lee, Membrane protein nanoparticles: the shape of things to come, Biochem. Soc. Trans. 46 (2018) 1495–1504.
[43] S. Gulati, M. Jamshad, T.J. Knowles, K.A. Morrison, R. Downing, N. Cant, R. Collins, J.B. Koenderink, R.C. Ford, M. Overduin, et al., Detergent-free purification of ABC (ATP-binding-cassette) transporters, Biochem. J. 461 (2014) 269–278.
[44] L. Shi, Q.-T. Shen, A. Kiel, J. Wang, H.-W. Wang, T.J. Melia, J.E. Rothman, F. Pincet, SNARE proteins: one to fuse and three to keep the nascent fusion pore open, Science 335 (6074) (2012) 1355–1359.
[45] B.C. Schroeder, S. Waldegger, S. Fehr, M. Bleich, R. Warth, R. Greger, T. J. Jentsch, A constitutively open potassium channel formed by KCNQ1 and KCNE3, Nature 403 (6766) (2000) 196–199.
[46] A. Lewis, Z.A. McCrossan, Abbott, G.W. MinK, MiRP1, and MiRP2 diversify Kv3.1 and Kv3.2 potassium channel gating, J. Biol. Chem. 279 (9) (2004) 7884–7892.
[47] B.M. Kroncke, W.D. Van Horn, J. Smith, C.B. Kang, R.C. Welch, Y.L. Song, D. P. Nannemann, K.C. Taylor, N.J. Sisco, A.L. George, et al., Structural basis for KCNE3 modulation of potassium recycling in epithelia, Sci. Adv. 2 (9) (2016), e1501228.
[48] G.W. Abbott, KCNE1 and KCNE3: the yin and yang of voltage-gated K+ channel regulation, Gene 576 (1) (2016) 1–13.
[49] R. Barro-Soria, R. Ramentol, S.I. Liin, M.E. Perez, R.S. Kass, H.P. Larsson, KCNE1 and KCNE3 modulate KCNQ1 channels by affecting different gating transitions, Proc. Natl. Acad. Sci. U. S. A. 114 (35) (2017) E7367–E7376.
[50] S. Ohno, F. Toyoda, D.P. Zankov, H. Yoshida, T. Makiyama, K. Tsuji, T. Honda, K. Obayashi, H. Ueyama, W. Shimizu, et al., Novel KCNE3 mutation reduces repolarizing potassium current and associated with long QT syndrome, Hum. Mutat. 30 (4) (2009) 557–563.
[51] P. Preston, L. Wartosch, D. Gunzel, M. Fromm, P. Kongsuphol, J. Ousingsawat, K. Kunzelmann, J. Barhanin, R. Warth, T.J. Jentsch, Disruption of the K+ channel beta-subunit KCNE3 reveals an important role in intestinal and tracheal cl-transport, J. Biol. Chem. 285 (10) (2010) 7165–7175.
[52] A. Boucherot, R. Schreiber, K. Kunzelmann, Regulation and properties of KCNQ1 (K(v)LQT1) and impact of the cystic fibrosis transmembrane conductance regulator, J. Membr. Biol. 182 (1) (2001) 39–47.
[53] A. Lundby, L.S. Ravn, J.H. Svendsen, S. Haunso, S.P. Olesen, N. Schmitt, KCNE3 mutation V17M identified in a patient with lone atrial fibrillation, Cell. Physiol. Biochem. 21 (1–3) (2008) 47–54.
[54] G.W. Abbott, M.H. Butler, S.A.N. Goldstein, Phosphorylation and protonation of neighboring MiRP2 sites: function and pathophysiology of MiRP2-Kv3.4 potassium channels in periodic paralysis, FASEB J. 20 (2) (2006) 293–301.
[55] E. Delpon, J.M. Cordeiro, L. Nunez, P.E.B. Thomsen, A. Guerchicoff, G. D. Pollevick, Y.S. Wu, J.K. Kanters, C.T. Larsen, E. Burashnikov, et al., Functional effects of KCNE3 mutation and its role in the development of Brugada syndrome, Circul.-Arrhyth. Electrophysiol. 1 (3) (2008) 209–218.
[56] D.F. Zhang, B. Liang, J. Lin, B. Liu, Q.S. Zhou, Y.Q. Yang, KCNE3 R53H substitution in familial atrial fibrillation, Chin. Med. J. 118 (20) (2005) 1735–1738.
[57] C.B. Kang, C.G. Vanoye, R.C. Welch, W.D. Van Horn, C.R. Sanders, Functional delivery of a membrane protein into oocyte membranes using bicelles, Biochemistry 49 (4) (2010) 653–655.

[58] P.J. Barrett, Y. Song, W.D. Van Horn, E.J. Hustedt, J.M. Schafer, A. Hadziselimovic, A.J. Beel, C.R. Sanders, The amyloid precursor protein has a flexible transmembrane domain and binds cholesterol, Science 336 (2012) 6085.

[59] I.D. Sahu, B.M. Kroncke, R. Zhang, M.M. Dunagan, H.J. Smith, A. Craig, R. M. McCarrick, C.R. Sanders, G.A. Lorigan, Structural investigation of the transmembrane domain of KCNE1 in Proteoliposomes, Biochemistry 53 (2014) 6392–6401.

[60] R. Zhang, I.D. Sahu, K.R. Gibson, N. Muhammad, A.P. Bali, R.G. Comer, L. Liu, A. F. Craig, R.M. McCarrick, C. Dabney-Smith, et al., Development of Electron spin Echo envelope modulation (ESEEM) spectroscopy to probe the secondary structure of recomninant membrane proteins in lipid bilayer, Protein Sci. 24 (2015) 1707–1713.

[61] O.V. Nolandt, T.H. Walther, S.L. Grage, A.S. Ulrich, Magnetically oriented dodecylphosphocholine bicelles for solid-state NMR structure analysis, Biochim. Biophys. Acta-Biomembr. 1818 (5) (2012) 1142–1147.

[62] G. Jeschke, DEER distance measurements on proteins, Annu. Rev. Phys. Chem. 63 (2012) 419–446.

[63] E.A. Feldmann, S. Ni, I.D. Sahu, C.H. Mishler, D.D. Risser, J.L. Murakami, S. K. Tom, R.M. McCarrick, G.A. Lorigan, B.S. Tolbert, et al., Evidence for direct binding between HetR from Anabaena sp PCC 7120 and PatS-5, Biochemistry 50 (43) (2011) 9212–9224.

[64] G. Jeschke, V. Chechik, P. Ionita, A. Godt, H. Zimmermann, J. Banham, C. R. Timmel, D. Hilger, H. Jung, DeerAnalysis2006 - a comprehensive software package for analyzing pulsed ELDOR data, Appl. Magn. Reson. 30 (3–4) (2006) 473–498.

[65] Y.W. Chiang, P.P. Borbat, J.H. Freed, The determination of pair distance distributions by pulsed ESR using Tikhonov regularization, J. Magn. Reson. 172 (2005) 279–295.

[66] D.J. Schneider, J.H. Freed, Calculating slow motional magnetic resonance spectra: a user's guide, in: L.J. Berlinger (Ed.), Biological Magnetic Resonance, Plenum Publishing, 1989.

[67] D.E. Budil, S. Lee, S. Saxena, J.H. Freed, Nonlinear-least-squares analysis of slow-motion EPR spectra in one and two dimensions using a modified Levenberg–Marquardt algorithm, J. Mag. Reson. Ser. A 120 (1996) 155–189.

[68] I.D. Sahu, A.F. Craig, M.M. Dunagan, K.R. Troxel, R. Zhang, A.G. Meiberg, C. N. Harmon, R.M. MaCarrick, B.M. Kroncke, C.R. Sanders, et al., Probing structural dynamics and topology of the KCNE1 membrane protein in lipid bilayers via site-directed spin labeling and Electron paramagnetic resonance spectroscopy, Biochemistry 54 (2015) 6402–6412.

[69] J.C. Phillips, R. Braun, W. Wang, J. Gumbart, E. Tajkhorshid, E. Villa, C. Chipot, R.D. Skeel, L. Kalé, K. Schulten, Scalable molecular dynamics with NAMD, J. Comput. Chem. 26 (2005) 1781–1802.

[70] A.D. MacKerell, D. Bashford, M. Bellott, R.L. Dunbrack, J.D. Evanseck, M.J. Field, S. Fischer, J. Gao, H. Guo, S. Ha, et al., All-atom empirical potential for molecular modeling and dynamics studies of proteins, J. Phys. Chem. B 102 (18) (1998) 3586–3616.

[71] A.D. MacKerell, M. Feig, C.L. Brooks, Improved treatment of the protein backbone in empirical force fields, J. Am. Chem. Soc. 126 (3) (2004) 698–699.

[72] S. Jo, T. Kim, V.G. Iyer, W. Im, Software news and updates - CHARNIM-GUI: A web-based grraphical user interface for CHARMM, J. Comput. Chem. 29 (11) (2008) 1859–1865.

[73] W. Humphrey, A. Dalke, K. Schulten, VMD-visual molecular dynamics, J. Mol. Graph. 14 (1) (1996) 33–38.

[74] C.D. Schwieters, G.M. Clore, The VMD-XPLOR visualization package for NMR structure refinement, J. Magn. Reson. 149 (2) (2001) 239–244.

[75] S. Jo, T. Kim, W. Im, Automated builder and database of protein/membrane complexes for molecular dynamics simulations, PLoS One 2 (9) (2007), e880.

[76] T.A. Ramelot, Y. Yang, I.D. Sahu, H.-W. Lee, R. Xiao, G.A. Lorigan, G. T. Montelione, M.A. Kennedy, NMR structure and MD simulations of the AAA protease intermembrane space domain indicates peripheral membrane localization within the hexaoligomer, FEBS Lett. 587 (21) (2013) 3522–3528.

[77] U. Essmann, L. Perera, M.L. Berkowitz, T. Darden, H. Lee, L.G. Pedersen, A smooth particle mesh ewald method, J. Chem. Phys. 103 (19) (1995) 8577–8593.

[78] R. Zhang, I.D. Sahu, L. Liu, A. Osatuke, R.G. Corner, C. Dabney-Smith, G. A. Lorigan, Characterizing the structure of lipodisq nanoparticles for membrane protein spectroscopic studies, Biochim. Biophys. Acta-Biomembr. 1848 (1) (2015) 329–333.

[79] A.F. Craig, E.E. Clark, I.D. Sahu, R. Zhang, N.D. Frantz, S. Al-Abdul-Wahid, C. Dabney-Smith, D. Konkolewicz, G.A. Lorigan, Tuning the size of styrene-maleic acid copolymer-lipid nanoparticles (SMALPs) using RAFT polymerization for biophysical studies, Biochim. Biophys. Acta 1858 (2016) 2931–2939.

[80] R. Zhang, I.D. Sahu, A.P. Bali, C. Dabney-Smith, G.A. Lorigan, Characterization of the structure of Lipodisq nanoparticles in the presence of KCNE1 by dynamic light scattering and transmission Electron microscopy, Chem. Phys. Lipids 203 (2016) 19–23.

[81] I.D. Sahu, R. Zhang, M.M. Dunagan, A. Craig, A., L. G., Characterization of KCNE1 inside lipodisq nanoparticles for EPR spectroscopic studies of membrane proteins, J. Phys. Chem. B 121 (21) (2017) 5312–5321.

[82] I.D. Sahu, A.F. Craig, M.M. Dunagum, R.M. McCarrick, G.A. Lorigan, Characterization of bifunctional spin labels for investigating the structural and dynamic properties of membrane proteins using EPR spectroscopy, J. Phys. Chem. B 121 (39) (2017) 9185–9195.

[83] A.T. Coey, I.D. Sahu, T.S. Gunasekera, K.R. Troxel, J.M. Hawn, M.S. Swartz, M. R. Wickenheiser, R.J. Reid, R.C. Welch, C.G. Vanoye, et al., Reconstitution of KCNE1 into lipid bilayers: comparing the structural, dynamic, and activity differences in micelle and vesicle environments, Biochemistry 50 (50) (2011) 10851–10859.

[84] Y. Song, E.J. Hustedt, S. Brandon, C.R. Sanders, Competition between Homodimerization and cholesterol binding to the C99 domain of the amyloid precursor protein, Biochemistry 52 (30) (2013) 5051–5064.

[85] G. Dixit, I.D. Sahu, W.D. Reynolds, T.M. Wadsworth, B.D. Harding, C.K. Jaycox, C. Dabney-Smith, C.R. Sanders, G.A. Lorigan, Probing the dynamics and structural topology of the reconstituted human KCNQ1 voltage sensor domain (Q1-VSD) in lipid bilayers using Electron paramagnetic resonance spectroscopy, Biochemistry 58 (7) (2019) 965–973.

[86] P.J. Barrett, Y. Song, W.D. Van Horn, E.J. Hustedt, J.M. Schafer, A. Hadziselimovic, A.J. Beel, C.R. Sanders, The amyloid precursor protein has a flexible transmembrane domain and binds cholesterol, Science 336 (6085) (2012) 1168–1171.

[87] I.D. Sahu, A.F. Craig, M.M. Dunagan, K.R. Troxel, R. Zhang, A.G. Meiberg, C. N. Harmon, R.M. MaCarrick, B.M. Kroncke, C.R. Sanders, et al., Probing structural dynamics and topology of the KCNE1 membrane protein in lipid bilayers via site-directed spin labeling and Electron paramagnetic resonance spectroscopy, Biochemistry 54 (41) (2015) 6402–6412.

[88] I.D. Sahu, G.A. Lorigan, Site-directed spin labeling EPR for studying membrane proteins, Biomed. Res. Int. 2018 (2018) 3248289.

[89] G. Jeschke, A. Bender, T. Schweikardt, G. Panek, H. Decker, H. Paulsen, Localization of the N-terminal domain in light-harvesting chlorophyll a/b protein by EPR measurements, J. Biol. Chem. 280 (19) (2005) 18623–18630.

[90] H.S. Mchaourab, E. Perozo, Determination of protein folds and conformational dynamics using spin-labeling EPR spectroscopy, in: L. Berliner, G. Eaton, S. Eaton (Eds.), Biol. Magn. Reson. Vol. 19, Springer, 2002, pp. 185–247.

[91] E. Perozo, D.M. Cortes, L.G. Cuello, Three-dimensional architecture and gating mechanism of a K+ channel studied by EPR spectroscopy, Nat. Struct. Biol. 5 (6) (1998) 459–469.

[92] V. Vasquez, M. Sotomayor, D.M. Cortes, B. Roux, K. Schulten, E. Perozo, Three-dimensional architecture of membrane-embedded MscS in the closed conformation, J. Mol. Biol. 378 (1) (2008) 55–70.

[93] I.D. Sahu, G.A. Lorigan, Electron paramagnetic resonance as a tool for studying membrane proteins, Biomolecules 10 (2020) 763.

[94] T. Ahammad, D.L. Drew, R.H. Khan, I.D. Sahu, E. Faul, T. Li, G.A. Lorigan, Structural dynamics and topology of the inactive form of S21 Holin in a lipid bilayer using continuous-wave Electron paramagnetic resonance spectroscopy, J. Phys. Chem. B 124 (2020) 5370–5379.

[95] T. Ahammad, D.L. Drew Jr., I.D. Sahu, R.A. Serafin, K.R. Clowes, G.A. Lorigan, Continuous wave electron paramagnetic resonance spectroscopy reveals the structural topology and dynamic properties of active pinholin $S2^{16}8$ in a lipid bilayer, J. Phys. Chem. B 123 (2019) 8048–8056.

[96] Y. Tkachev, V. Timofeev, Uniform EPR spectra analysis of spin-labeled macromolecules by temperature and viscosity dependences, in: A.I. Kokorin (Ed.), Nitroxides - Theory, Experiment and Applications Intech, 2012, pp. 285–314.

[97] W. Fan, R.M. Evans, Turning up the heat on membrane fluidity, Cell 161 (5) (2015) 962–963.

[98] L. Columbus, W.L. Hubbell, A new spin on protein dynamics, Trends Biochem. Sci. 27 (2002) 288–295.

[99] J.M. Isas, R. Langen, H.T. Haigler, W.L. Hubbell, Structure and dynamics of a helical hairpin and loop region in annexin 12: A site-directed spin labeling study, Biochemistry 41 (5) (2002) 1464–1473.

[100] C. Campbell, F.D.M. Faleel, M.W. Scheyer, S. Haralu, P.L. Williams, W.D. Carbo, A.S. Wilson-Taylor, N.H. Patel, C.R. Sanders, G.A. Lorigan, et al., Comparing the structural dynamics of the human KCNE3 in reconstituted micelle and lipid bilayered vesicle environments, Biochim. Biophys. Acta-Biomembr. 1864 (10) (2022), 183974.

[101] D.T. Warshaviak, V.V. Khramtsov, D. Cascio, C. Altenbach, W.L. Hubbell, Structure and dynamics of an imidazoline nitroxide side chain with strongly hindered internal motion in proteins, J. Magn. Reson. 232 (2013) 53–61.

[102] M.R. Fleissner, M.D. Bridges, E.K. Brooks, D. Cascio, T. Kálai, K. Hideg, W. L. Hubbell, Structure and dynamics of a conformationally constrained nitroxide side chain and applications in EPR spectroscopy, Proc. Natl. Acad. Sci. U. S. A. 108 (39) (2012) 16241–16246.

[103] J.E. McCaffrey, Z.M. James, B. Svensson, B.P. Binder, D.D. Thomas, A bifunctional spin label reports the structural topology of phospholamban in magnetically-aligned bicelles, J. Magn. Reson. 262 (2016) 50–56.

[104] P.P. Borbat, H.S. McHaourab, J.H. Freed, Protein structure determination using long-distance constraints from double-quantum coherence ESR: study of T4 lysozyme, J. Am. Chem. Soc. 124 (2002) 5304–5314.

[105] G. Jeschke, Y. Polyhach, Distance measurements on spin-labelled biomacromolecules by pulsed electron paramagnetic resonance, Phys. Chem. Chem. Phys. 9 (16) (2007) 1895–1910.

[106] C.C. Jao, B.G. Hegde, J. Chen, I.S. Haworth, R. Langen, Structure of membrane-bound alpha-synuclein from site-directed spin labeling and computational refinement, Proc. Natl. Acad. Sci. U. S. A. 105 (50) (2008) 19666–19671.

[107] A. Mokdad, D.Z. Herrick, A.K. Kahn, E. Andrews, M. Kim, D.S. Cafiso, Ligand-induced structural changes in the Escherichia coli ferric citrate transporter reveal modes for regulating protein-protein interactions, J. Mol. Biol. 423 (5) (2012) 818–830.

[108] O. Schiemann, P. Cekan, D. Margraf, T.F. Prisner, S.T. Sigurdsson, Relative orientation of rigid nitroxides by PELDOR: beyond distance measurements in nucleic acids, Angew. Chem.-Intern. Ed. 48 (18) (2009) 3292–3295.

[109] B. Endeward, J.A. Butterwick, R. MacKinnon, T.F. Prisner, Pulsed Electron-Electron double-resonance determination of spin-label distances and orientations

on the tetrameric potassium Ion Channel KcsA, J. Am. Chem. Soc. 131 (42) (2009) 15246–15250.
[110] G. Jeschke, C. Wegener, M. Nietschke, H. Jung, H.J. Steinhoff, Interresidual distance determination by four-pulse double electron-electron resonance in an integral membrane protein: the Na+/proline transporter PutP of Escherichia coli, Biophys. J. 86 (4) (2004) 2551–2557.
[111] D. Hilger, H. Jung, E. Padan, C. Wegener, K.P. Vogel, H.J. Steinhoff, G. Jeschke, Assessing oligomerization of membrane proteins by four-pulse DEER: pH-dependent dimerization of NhaA Na+/H+ antiporter of E-coli, Biophys. J. 89 (2) (2005) 1328–1338.
[112] D. Hilger, Y. Polyhach, E. Padan, H. Jung, G. Jeschke, High-resolution structure of a Na+/H+ antiporter dimer obtained by pulsed election paramagnetic resonance distance measurements, Biophys. J. 93 (2007) 3675–3683.
[113] Q. Xu, J.F. Ellena, M. Kim, D.S. Cafiso, Substrate-dependent unfolding of the energy coupling motif of a membrane transport protein determined by double electron-electron resonance, Biochemistry 45 (36) (2006) 10847–10854.
[114] P. Stepien, A. Polit, A. Wisniewska-Becker, Comparative EPR studies on lipid bilayer properties in nanodiscs and liposomes, Biochim. Biophys. Acta-Biomembr. 1848 (1) (2015) 60–66.
[115] M. Jamshad, V. Grimard, I. Idini, T.J. Knowles, M.R. Dowle, N. Schofield, P. Sridhar, Y. Lin, R. Finka, M. Wheatley, et al., Structural analysis of a nanoparticle containing a lipid bilayer used for detergent-free extraction of membrane proteins, Nano Res. 8 (3) (2015) 774–789.
[116] S.S. Kim, M.A. Upshur, K. Saotome, I.D. Sahu, R.M. McCarrick, J.B. Feix, G. A. Lorigan, K.P. Howard, Cholesterol-dependent conformational exchange of the C-terminal domain of the influenza A M2 protein, Biochemistry 54 (49) (2015) 7157–7167.
[117] K.A. Morrison, A. Akram, A. Mathews, Z.A. Khan, J.H. Patel, C.M. Zhou, D. J. Hardy, C. Moore-Kelly, R. Patel, V. Odiba, et al., Membrane protein extraction and purification using styrene-maleic acid (SMA) copolymer: effect of variations in polymer structure, Biochem. J. 473 (2016) 4349–4360.
[118] V.A. Bjornestad, M. Orwick-Rydmark, R. Lund, Understanding the structural pathways for lipid Nanodisc formation: how styrene maleic acid copolymers induce membrane fracture and disc formation, Langmuir 37 (20) (2021) 6178–6188.
[119] E. Kamilar, J. Bariwal, W. Zheng, H.R. Ma, H.J. Liang, SMALPs are not simply nanodiscs: the polymer-to-lipid ratios of fractionated SMALPs underline their heterogeneous nature, Biomacromolecules 24 (4) (2023) 1819–1838.
[120] S.K. Kandasamy, R.G. Larson, Molecular dynamics simulations of model trans-membrane peptides in lipid bilayers: A systematic investigation of hydrophobic mismatch, Biophys. J. 90 (7) (2006) 2326–2343.
[121] B.D. Harding, G. Dixit, K.M. Burridge, I.D. Sahu, C. Dabney-Smith, R.E. Edelmann, D. Konkolewicz, G.A. Lorigan, Characterizing the structure of styrene-maleic acid copolymer-lipid nanoparticles (SMALPs) using RAFT polymerization for membrane protein spectroscopic studies, Chem. Phys. Lipids 218 (2019) 65–72.
[122] A.P. Bali, I.D. Sahu, A.F. Craig, E.E. Clark, K.M. Burridge, M.T. Dolan, C. Dabney-Smith, D. Konkolewicz, G.A. Lorigan, Structural characterization of styrene-maleic acid copolymer-lipid nanoparticles (SMALPs) using EPR spectroscopy, Chem. Phys. Lipids 220 (2019) 6–13.
[123] K.M. Burridge, B.D. Harding, I.D. Sahu, M.M. Kearns, R.B. Stowe, M.T. Dolan, R. E. Edelmann, C. Dabney-Smith, R.C. Page, D. Konkolewicz, et al., Simple derivatization of RAFT-synthesized styrene-maleic anhydride copolymers for lipid disk formulations, Biomacromolecules 21 (3) (2020) 1274–1284.
[124] A.F. Craig, E.E. Clark, I.D. Sahu, R. Zhang, N.D. Frantz, S. Al-Abdul-Wahid, C. Dabney-Smith, D. Konkolewicz, G.A. Lorigan, Tuning the size of styrene-maleic acid copolymer-lipid nanoparticles (SMALPs) using RAFT polymerization for biophysical studies, Biochim. Biophys. Acta 1858 (2016) 2931–2939.
[125] G.M. Di Mauro, C. La Rosa, M. Condorelli, A. Ramamoorthy, Benchmarks of SMA-copolymer derivatives and Nanodisc integrity, Langmuir 37 (10) (2021) 3113–3121.